

On the Computational Cost of Stochastic Security

Noah A. Crum,^{1,*} Leanto Sunny,^{1,†} Pooya Ronagh,^{2,3,4,5,‡}
Raymond Laflamme,^{2,3,4,§} Radhakrishnan Balu,^{6,7,¶} and George Siopsis^{1,**}

¹*Department of Physics & Astronomy, The University of Tennessee, Knoxville, TN 37996-1200, USA*

²*Institute for Quantum Computing, University of Waterloo, Waterloo, ON, N2L 3G1, Canada*

³*Department of Physics & Astronomy, University of Waterloo, Waterloo, ON, N2L 3G1, Canada*

⁴*Perimeter Institute for Theoretical Physics, Waterloo, ON, N2L 2Y5, Canada*

⁵*1QB Information Technologies (1QBit), Vancouver, BC, V6E 4B1, Canada*

⁶*Computer & Information Sciences Directorate, Army Research Laboratory, Adelphi, MD 21005-5069, USA*

⁷*Department of Mathematics, University of Maryland, College Park, MD 20742-4015, USA*

(Dated: May 16, 2023)

We investigate whether long-run persistent chain Monte Carlo simulation of Langevin dynamics improves the quality of the representations achieved by energy-based models (EBM). We consider a scheme wherein Monte Carlo simulation of a diffusion process using a trained EBM is used to improve the adversarial robustness and the calibration score of an independent classifier network. Our results show that increasing the computational budget of Gibbs sampling in persistent contrastive divergence improves the calibration and adversarial robustness of the model, elucidating the practical merit of realizing new quantum and classical hardware and software for efficient Gibbs sampling from continuous energy potentials.

I. INTRODUCTION

A recent reincarnation of energy-based models (EBM) has provided state-of-the-art performance in generative modeling [1–3], and has been suggestive of improved representation of data in measures such as robustness of the model to adversarial attacks and calibrated prediction [2, 4]. However, sampling from the canonical distribution represented by the model, which – via inspirations from statistical mechanics – is the Gibbs distribution of an energy potential represented by the model, remains the main computational bottleneck in seamless training of EBMs.

Conventional EBMs, such as the Boltzmann machines and Hopfield neural networks [5, 6], and their derivative models [7, 8], are built via undirected graphical models [9, 10]. The neurons represent discrete (binary) random variables and the energy of the model is a function of these discrete random variables (for example, a quadratic binary-valued function representing two-body interactions between the neurons). However, modern EBMs use deep neural networks as their underlying graphical model. The deep neural network parametrizes a highly non-convex energy potential defined on a continuous domain (i.e., the continuous input signals provided to the input neurons of the deep neural network).

Such EBMs are trained using Monte Carlo integration of Langevin dynamics [1, 11] – a stochastic differential equation (SDE) governing diffusion processes. Alternatively,

corrections using the Metropolis-Hastings criteria [12], and second-order variations, such as the Hamiltonian Monte Carlo [13], can be used. Regardless, these methods for Gibbs sampling are extremely costly, numerically unstable, and typically suffer from exponentially long mixing time. Indeed, many of the prior art use non-convergent shortcuts to training EBMs by collecting short-run Langevin samples [14]. The number of Langevin steps (i.e., the Monte Carlo iterations on the SDE) required for training truly convergent EBMs is expected to be at least in the tens of thousands even for small resolution image data [11].

Simulating equilibrium dynamics has been speculated as a potential application of quantum computers for the past two decades [15–21]. But these references focus on Gibbs sampling from discrete spin systems, limiting their application to traditional EBMs [22–26]. Consequently, more recent articles investigate quantum advantage in Gibbs sampling on continuous domains, namely [27] relying on quantum random walks but confining to convex potentials, and [28] by solving the Fokker–Planck partial differential equation (PDE) for non-convex periodic potentials. The Fokker–Planck equation (FPE) is the PDE counterpart to the Langevin SDE via the Feynman-Kac formula [29]. These quantum algorithms require large-scale fault-tolerant quantum computers to train a model with as many parameters as a modest size modern EBM. Therefore, it is crucial to ask whether a prospective quantum acceleration of continuous domain Gibbs sampling can act as a practical motivation for building large fault-tolerant quantum computers. We refer the reader to Section II for more details on classical and quantum algorithms for training EBMs.

Adversarial vulnerability is a critical obstacle for reliable deployment of autonomous agents in sensitive decision making scenarios. References [1] and [2] show that EBMs trained via Langevin dynamics exhibit adversarial

* ncrum@vols.utk.edu

† lsunny@vols.utk.edu

‡ pooya.ronagh@uwaterloo.ca

§ laflamme@uwaterloo.ca

¶ rbalu@umd.edu

** siopsis@tennessee.edu

robustness without explicit adversarial training. It is also important that the agent be aware of its degree of confidence in its decision; it is prudent that they recognize scenarios in which interjection from human domain experts is required. While conventional supervised learning models have grown increasingly accurate in their predictive ability, they have turned less and less calibrated [30] in their representations. In contrast, [2] shows that EBMs can learn highly calibrated representations of the CIFAR-10 and CIFAR-100 datasets. Other proposed advantages of EBMs include improved mode coverage [1] and better out-of-distribution (OOD) detection [1, 2] compared to the autoregressive and flow generative models.

In this paper, we investigate the scaling of two utility parameters, namely, the adversarial robustness and the calibration scores of EBMs, with respect to the computational budget allowed for stochastic gradient Langevin dynamics (SGLD) iterations during training. Following [4], diffusion of the image using the energy potential represented by a trained EBM is used to purify an image from adversarial attacks before presenting the image to a classifier network. As will be shown, it turns out that the same diffusion process can also result in more calibrated logits for the classifier. We train a wide residual network (WRN) 28-10 classifier [31], and a plurality of EBMs using variable numbers of SGLD steps. Our results show that purification of samples using EBMs trained with larger numbers of SGLD steps improves both the adversarial robustness and the calibration of the WRN classifier. We visually observe exponential decays in adversarial vulnerability and calibration error of the WRN and quantify these trend using linear regression. Our results provide positive evidence for utility of efficient Gibbs samplers from continuous potentials, making the case that the computational bottleneck of EBMs is one that is worth overcoming using quantum computation.

II. ENERGY-BASED MODELS

An EBM comprises a graphical model that acts as a function approximator for an *energy potential* $E_\theta : \Omega \rightarrow \mathbb{R}$. Here $\theta \in \mathbb{R}^d$ denotes a vector of model parameters for a model with d parameters, $\Omega \subseteq \mathbb{R}^D$ is a probability space endowed with a probability measure, and D is the dimension of input signals. In this paper we focus on image data; therefore, D is the number of pixels of the images multiplied by its number of color channels. We also assume pixel intensities normalized between 0 and 1, and therefore $\Omega = [0, 1]^D$ throughout.

Similar to other ML models, the graphical model is used to determine a *model distribution*. Given a set of i.i.d training samples $\mathcal{D} = \{x_1, \dots, x_N\} \subset \Omega$ the goal of the learning procedure is to find a vector of model parameters $\theta^* \in \mathbb{R}^d$ such that the corresponding model distribution best approximates an unknown distribution p from which \mathcal{D} is assumed to have been sampled from.

What is specific about EBMs is that the model distributions are Gibbs distribution

$$p_\theta(x) = \exp(-\beta E_\theta(x)) / Z_{\beta, \theta} \quad (1)$$

of the energy potential. The normalizing constant $Z_{\beta, \theta} = \int_{x \in \Omega} \exp(-\beta E_\theta(x)) dx$ is the partition function of p_θ at thermodynamic constant β .

Since the model only determines the energy potential E_θ (and not p_θ directly) it is called an *unnormalized* probabilistic graphical model. Unlike typical ML models used in discriminative tasks such as classification, EBMs do not impose any limitations on the model to assure tractability of the normalization constant. As a result EBMs are more expressive, however, this comes at the cost of computational intractability of the training of the model and inference from it.

The standard method for training probabilistic models from i.i.d. data is maximum likelihood training; i.e., maximizing the expected log-likelihood function over the data distribution, $\mathbb{E}_{x \sim p}[\log p_\theta(x)]$. This is equivalent to minimizing the KL distance between p_θ and p since

$$d_{\text{KL}}(p(x) || p_\theta(x)) = -\mathbb{E}_{x \sim p}[\log p_\theta(x)] + \text{constant}. \quad (2)$$

Actually, we do not need access to the value of the likelihood directly but rather the gradient of the log-probability of the model. This is the case at least for first-order optimization schemes which are the standard techniques for training classical ML models. We have

$$\begin{aligned} \nabla_\theta \log p_\theta(x) &= -\beta \nabla_\theta E_\theta(x) - \nabla_\theta \log Z_{\theta, \beta} \\ &= -\beta \nabla_\theta E_\theta(x) + \beta \mathbb{E}_{x \sim p_\theta}[\nabla_\theta E_\theta(x)]. \end{aligned} \quad (3)$$

In EBMs the first term above is easy to calculate through automatic differentiation but the second term is approximated through costly Gibbs sampling. Indeed, if we can draw samples from the model distribution p_θ , we have access to unbiased estimates of $\nabla_\theta E_\theta(x)$, which in turn can be used to train the EBM via stochastic gradient descent. The overdamped Langevin diffusion

$$dx = -\alpha \nabla_x E_\theta(x) dt + \sigma dW \quad (4)$$

where W is a standard Wiener process is known to mix into the Gibbs distribution of interest to us at inverse temperature $\beta = 2\alpha/\sigma^2$. Monte Carlo simulation of this SDE is known as stochastic gradient Langevin dynamics (SGLD) and amounts to building discrete time chains

$$\begin{aligned} x_0 &\sim p_0(x), \\ x_{i+1} &= x_i - \alpha \nabla E_\theta(x_i) dt + \varepsilon_i, \quad \varepsilon_i \sim N(0, \sigma), \end{aligned} \quad (5)$$

after a finite number of iterations, where the initial distribution p_0 is typically a uniform distribution.

A quantum Gibbs sampler can replace SGLD as explained in [28] and summarized here. The neural network of the EBM is a (white-box) composition of affine transformations with nonlinear activation functions. One can efficiently construct quantum circuits implementing

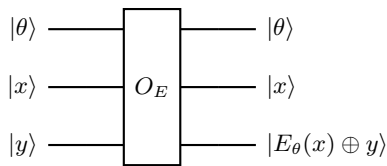


FIG. 1: The oracle for the energy potential. All registers receive float-point representations of real numbers. The first register receives the current model parameters $\theta \in \mathbb{R}^d$. The second register receives a data sample $x \in \Omega$. And, the third register is used to evaluate the energy potential.

the arithmetic required for realizing each such function [32] with only polylogarithmic overhead compared to the gate complexity of the corresponding classical boolean circuit. We can therefore construct a quantum oracle for the classical deep neural network endowed with a register for input samples $|x\rangle$ in the computational basis, and another register for receiving the model parameters $|\theta\rangle$. Fig. 1 provides a schematic representation of such an oracle. The algorithm of [28] works by queries to an oracle for the discretization of the generator of the FPE which itself is constructed using $O(D^2)$ replicas of the energy oracle in Fig. 1. Quantum Fourier transforms allow [28] to efficiently solve the FPE when the energy potential satisfies periodic boundary conditions. This algorithm provides polynomial and exponential quantum speedups in various factors and for various families of periodic potentials as explained in [28].

III. TRAINING WITH PERSISTENT CHAIN MONTE CARLO

We train a variety of EBMs on the CIFAR10 dataset [33] using SGLD as described in Section II. The training procedure uses persistent contrastive divergence (PCD) [34], wherein a replay buffer is used to retain samples from older shorter runs of Langevin dynamics. This persistent chain buffer offers orders of magnitude (perhaps more than thousands even for small datasets [11]) saving in the simulation time of stochastic Langevin dynamics but comes with the cost of increased training instability. Indeed, the distribution, π , representing the persistent chain is different from the true model distribution (the Gibbs distribution), p_θ . The update direction followed by θ deviates from that of (2) and must instead be viewed as

$$d_{\text{KL}}(p(x)||p_\theta(x)) - d_{\text{KL}}(\pi||p_\theta(x)). \quad (6)$$

Note that the second divergence is maximized during training. Therefore the persistent chain distribution diverges from the instantaneous Gibbs state during training, and the faster the model parameters are updated (i.e., with higher learning rate), this deviation increases.

Our empirical efforts made it evident that it is not quite feasible to train such EBMs without PCD. Since we do not reinitialize the persistent chain samples each

PCD sample experiences all the SGLD steps during the training which is proportional to the number of SGLD steps in each epoch of training. Despite the discrepancy (6), this number can be a good indicator of the computational cost of Gibbs sampling for training EBMs.

For our experiments we train five distinct EBMs using the lightweight architecture of [14], applying a different number of Langevin steps during PCD for each model. Each EBM is trained for 250,000 batches, beginning with the Adam optimizer [35] and switching to SGD after 125,000 batches with learning rates of 1e-4 and 5e-5 respectively. The change from Adam to SGD has been found to be essential for stable and convergent training of EBMs [14]. Details of the hyperparameters used in training the models in this paper can be found in Table I.

IV. ADVERSARIAL ROBUSTNESS

Following [4] we train a prototypical wide residual network (WRN) 28-10 classifier [31]. The classifier is trained for 100 epochs with a scheduled learning rate decay via SGD on a cross-entropy loss function, with an L_2 regularizer of coefficient 2e-4 for the weights and biases of the model. We denote the classification labels by $y \in \mathcal{Y} = \{1, \dots, 10\}$, and for an input image x we denote the output logits of the classifier by $f(x)$. We perform white-box projected gradient descent (PGD) attacks [36] on the classifier then we pass the attacked image through Langevin dynamics of the EBMs trained in Section II in order to purify the image from the attack. We refer the reader to [4, Appendix C] for some theoretical justifications on this method based on the memoryless or the chaotic behavior of Markov chain Monte Carlo sampling.

An adversarial attack on a classifier with output logits $f(x) \in \mathbb{R}^{|\mathcal{Y}|}$ searches for a sample $x \in [0, 1]^D$ in a neighborhood S of an attacked image x^+ that maximizes the cross-entropy loss:

$$x_{adv}(x^+, y) = \arg \max_{x \in S} L(f(x), y). \quad (7)$$

The cross-entropy loss $L(f(x), y)$ is $-\log(p_y)$ where p_y is the likelihood of the label y , obtained by passing $f(x)$

	WRN classifier	EBMs
Training Duration	100 epochs	250,000 batches
Batch size	100	100
Learning rates (LR)	[1e-1, 1e-2, 1e-3]	[1e-4, 5e-5]
LR switch time	epochs 40 and 60	batch 125,000
L_2 regularizer	2e-4	0
SGLD steps, n	-	[50, 75, 100, 150, 200]
SGLD step size, α	-	0.01
SGLD noise, σ	-	0.01

TABLE I: Training hyperparameters. First column pertains to training of the WRN classifier. The second column reflects the hyperparameters used for training EBMs with varied numbers of SGLD steps.

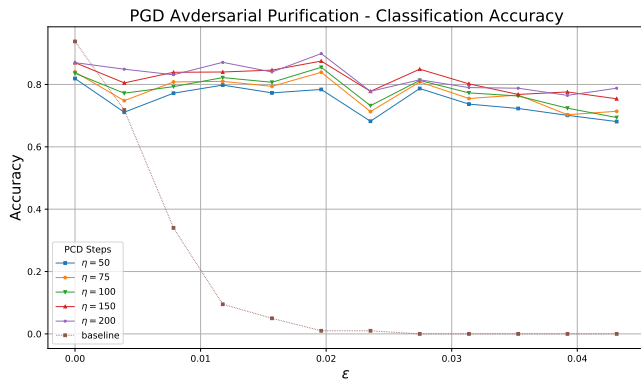


FIG. 2: Classification accuracy versus adversarial attack strength ε . The ‘baseline’ refers to the classifier unequipped with an EOT defense. The other curves represent the accuracy of the distinct EBMs at classification of 1000 PGD adversarial images post-transformation as a function of attack strength, ε .

through the softmax operator. S is an ε -ball around x^+ in the L_∞ -norm and we have assumed pixel intensities between 0 to 1 for images. A PGD attack starts from a random initial point in S and maximizes the above objective function via iterative advances along a steepest descent direction followed by projections back onto S . That is,

$$x_{i+1} = \Pi_S(x_i + \alpha g(x_i, y)), \quad \text{where} \\ g(x, y) = \arg \max_{\|v\|_\infty \leq 1} v^\top \Delta(x, y) = \text{sign}(\Delta(x, y)). \quad (8)$$

Here Π_S denotes the projection onto S , α is the attack step size, and $\Delta(x, y)$ is the attack gradient which is $\nabla_x L(f(x), y)$ in the notation above.

We generate 1000 adversarial images via PGD attacks on the classifier for various attack strengths $\varepsilon > 0$. These images are then diffused through the EBMs using 1500 Langevin steps for 150 parallel trials. The outputs are provided to the classifier and the logits of all the trials are averaged

$$F(x) \simeq \mathbb{E}_{T(x)}[f(T(x))] \quad (9)$$

to provide a final *post-transformation* label. Here $T(x)$ represents the random tensor produced after diffusion of x through Langevin dynamics. This procedure is known as the expectation over transformation (EOT) defense [4]. We perform this procedure using EBMs trained with different numbers of Langevin steps and demonstrate that longer Langevin sampling improves the adversarial robustness of this defense.

As shown in Fig. 2, the standalone classifier is severely vulnerable to PGD attacks while energy-based purification restores the majority of adversarial images to their original classification labels. In Fig. 3 we observe that an increase in the duration of Langevin dynamics during training of the EBM confers greater restorative power to the EBM, augmenting its capabilities of distilling the adversarial signals. We also regress an average exponential

decay rate in classification error across different choices of ε and as a function of the number of PCD steps.

The small rate of this decay suggests that achieving adversarial security may require training EBMs with very large numbers of SGLD steps. For further investigation, we also calculate the relative accuracy error of the defense compared to the original classification error of the model on clean images. Since the goal of the purification process is to restore adversarial classification accuracy to that of the classifier’s original accuracy on clean images, the relative error is ideally 1 indicating the classifier is equally successful at classification of clean images as it is with respect to adversarial classification post-transformation. Table II shows the predicted number of PCD steps, according to the linear fit in Fig. 3(b), needed during training to allow the EBM to restore the classifier’s performance on post-transformation adversarial images to that of the original classifier for each ε . We note that a projected runtime for a model utilizing 450 Langevin steps during training in the same fashion as our other models is approximately 3.25 days on a single Nvidia Tesla V100S GPU.

The EOT defense, itself, gives rise to one of the strongest attacks in the literature [37] known as the EOT attack, which exploits access to the classifier logits for a finite number m of i.i.d. attack samples $x_1, \dots, x_m \sim T(x)$ and the following approximation of $F(x)$:

$$\hat{F}_m(x) = \frac{1}{m} \sum_{i=1}^m f(\hat{x}_i). \quad (10)$$

Performing PGD attacks on these logits require access to derivatives of the diffusion process T which is overcome using *backward pass differentiable approximation* (BPDA) [37] which in this simplest case approximates the transformation T via the identity mapping. Therefore PGD will use $L(f(T(x), y))$ in the forward pass, but use $\nabla_x L(f(x), y)$ as the attack gradient in the backward pass. Together the EOT and BPDA give rise to the following attack gradient for PGD:

$$\Delta(x, y) = \frac{1}{m} \sum_{i=1}^m \nabla_{\hat{x}_i} L \left(\frac{1}{m} \sum_{i=1}^m f(\hat{x}_i, y) \right). \quad (11)$$

Performing BPDA+EOT attacks is computationally expensive, and therefore the results in Fig. 4 are restricted to the fixed attack strength of $\varepsilon = 8/255$ (a customary attack strength used in the literature for benchmarking). For these attacks, a baseline accuracy and prediction error are reported referring to the performance

$255 \times \varepsilon$	0	1	2	3	4	5	6	7	8	9	10	11
n	338	300	450	348	380	247	422	655	553	651	503	419

TABLE II: Projected SGLD step counts. For each attack strength ε , the reported value of n indicates the predicted number of SGLD steps required during training of the model to restore the classifier back to its original performance with respect to classification of the PGD adversarial images according to regression of a linear trend between the relative classification error versus number of SGLD steps in Fig. 3(b).

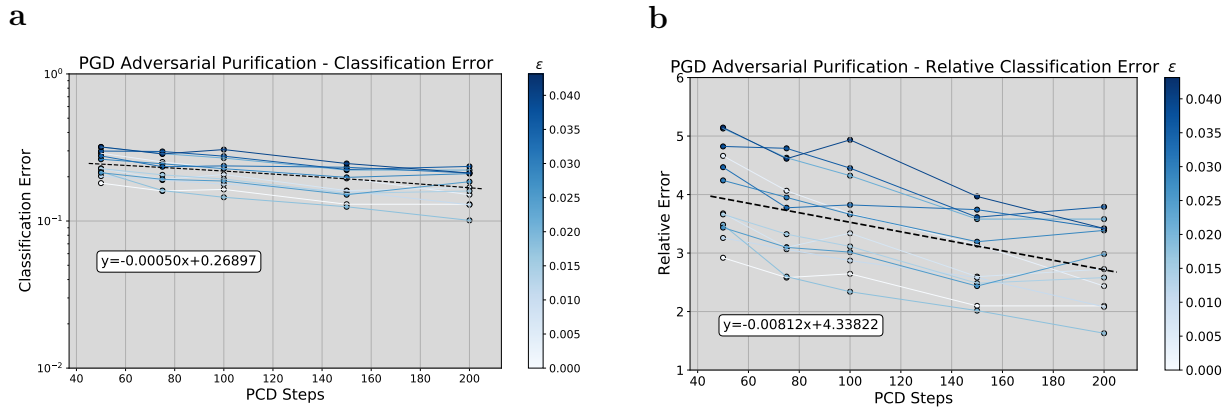


FIG. 3: (a) Post-transformation PGD classification error as a function of the number of SGLD steps of each iteration of training. (b) Error relative to the performance of the baseline classifier on clean images. The color shade of the curves indicate the strength, ϵ , of the applied PGD attack.

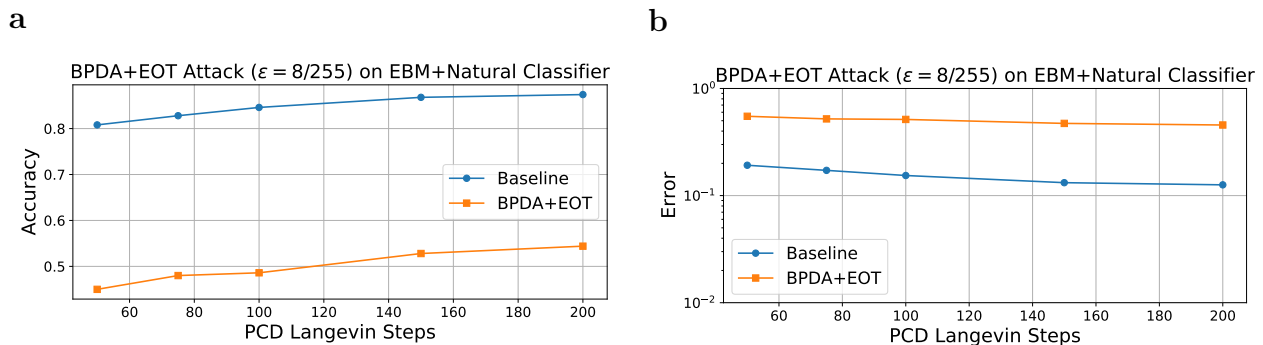


FIG. 4: (a) BPDA+EOT attack on the combination of the EBM and the WRN classifier as a function of SGLD steps used during training. ‘Baseline’ is the pre-attack accuracy, while the other curve shows the post-attack accuracy. The BPDA+EOT attack degrades the performance of the model, however, longer SGLD runs confer greater resistance to the attacks. (b) The classification error on a logarithmic scale as a function of the number of SGLD steps.

of the combination of each of the EBMs and the classifier pre-attack. We observe that the classification accuracy of the baseline model improves with longer runs of Langevin dynamics during training. The result of the BPDA+EOT attack are reported on the same plots. This attack results in a considerable reduction in classification performance of the joint model. Nevertheless, EBMs experiencing longer-run Langevin dynamics during training exhibit more resistance to this form of attack as well.

V. CALIBRATION OF THE MODEL

In addition to improved adversarial robustness, we provide numerical evidence supporting that prolonged PCD during the training of EBMs confer improvements to the calibration of the model as well. Specifically, we study the calibration in the classification of adversarial images, since calibration also pertains to classification capabilities and the standalone EBM is not a discriminative model. Calibration indicates that the model’s predictive confidence, $\max_y p(y|x)$, is commensurate with its misclassification rate. To calculate the expected calibration

error (ECE), we find the classification confidence of each sample x in the dataset, and group them into equally spaced bins, $\{B_m\}_{m=1}^M$. For example, with $M = 20$ bins, B_0 corresponds to all images for which the classifier’s confidence is between 0 and 0.05. ECE is therefore defined as

$$\text{ECE} = \sum_{m=1}^M \frac{|B_m|}{N} |\text{acc}(B_m) - \text{conf}(B_m)| \quad (12)$$

where N is in the number of examples in the dataset, and $\text{acc}(B_m)$ and $\text{conf}(B_m)$ are respectively the average accuracy and confidence for the samples in bin B_m .

Fig. 5 shows the ECE of the post-purification adversarial images as a function of the number of PCD steps for each PGD attack strength, ϵ . The slope of the trendline is indicative of a steady but slow improvement in the calibration error with an increase in the number of PCD steps.

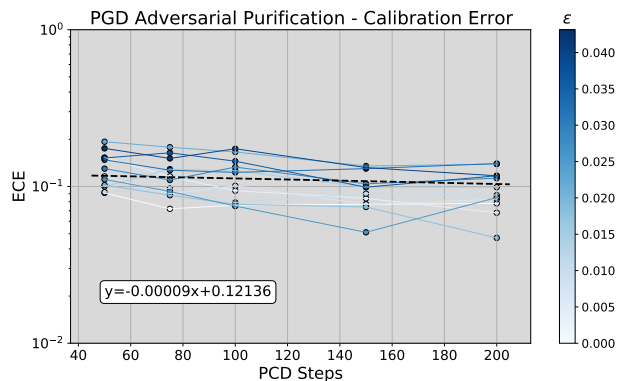


FIG. 5: Expected calibration error (ECE) as a function of the number of SGLD steps executed during the training of EBMs. The ECE calculation pertains to the post-transformation adversarial images. The color shade of the curves shows the strength of the applied PGD attack.

VI. CONCLUSION

A key missing element on the path to fault-tolerant quantum computation is practical utility measures that quantify how transformative the technology will be [38]. Quantum algorithms for solving differential equations can be used to simulate diffusion processes of interest in generative modeling [1, 2, 28, 39]. Also, it has been shown that the models trained in this fashion exhibit improved stochastic security [1, 2, 4]. Therefore, in this paper we propose stochastic security as a practical metric for gauging the utility of quantum Gibbs samplers in machine learning tasks.

Since diffusion processes provide the mathematical models of equilibrium and non-equilibrium thermodynamics, they play critical roles in machine learning. The high computational cost of the classical simulation of these processes, in terms of the time, energy, carbon and water footprint of training the models [40, 41] has encouraged machine learning scientists to pinpoint the practical benefits of training models that rely on them. In this paper we focused on deep energy-based models [1] (EBM) as an example from this family. We investigated two specific utility measures namely, the adversarial robustness and the calibration of EBMs. The EBMs were trained on classical image data using various amounts of computa-

tional budget allocated for performing stochastic gradient Langevin dynamics (SGLD) in order to simulate the diffusion process. After training, diffusion of a test image using the energy potential represented by the trained EBM is used as a transformation that purifies the image from the adversarial attack before presenting it to a wide residual network (WRN) classifier.

Our results show that the purification of samples using EBMs trained with larger numbers of SGLD steps improves the adversarial robustness of the WRN classifier. Interestingly, our experiments furthermore reveal that the same diffusive transformation also results in a more calibrated classification. We visually observe exponential decays in adversarial vulnerability and calibration error of the WRN and quantify these trend using linear regression. Our results provide a promising evidence for the practical utility of efficient quantum Gibbs samplers, making the case that even polynomially scaling quantum advantages in the precision of estimations of the observables of the Gibbs state directly contribute to improved stochastic security of ML models trained using quantum computers.

ACKNOWLEDGMENTS

This material is based upon work supported by the U.S. Department of Homeland Security through a contract with the Critical Infrastructure Resilience Institute (CIRI) at the University of Illinois. N. A. C., L. S., and G. S. acknowledge support by the U.S. Army Research Office under grant W911NF-19-1-0397 and the U.S. National Science Foundation under grant DGE-2152168. P. R. further acknowledges the support of NSERC Discovery grant RGPIN-2022-03339, Mike and Ophelia Lazaridis, Innovation, Science and Economic Development Canada (ISED), 1QBit, and the Perimeter Institute for Theoretical Physics. Research at the Perimeter Institute is supported in part by the Government of Canada through ISED, and by the Province of Ontario through the Ministry of Colleges and Universities. This research used resources of the Oak Ridge Leadership Computing Facility, which is a DOE Office of Science User Facility supported under Contract DE-AC05-00OR22725.

-
- [1] Y. Du and I. Mordatch, Implicit generation and generalization in energy-based models, arXiv preprint arXiv:1903.08689 (2019).
 - [2] W. Grathwohl, K.-C. Wang, J.-H. Jacobsen, D. Duvenaud, M. Norouzi, and K. Swersky, Your classifier is secretly an energy based model and you should treat it like one, arXiv preprint arXiv:1912.03263 (2019).
 - [3] Y. Song and D. P. Kingma, How to train your energy-based models, arXiv preprint arXiv:2101.03288 (2021).
 - [4] M. Hill, J. Mitchell, and S.-C. Zhu, Stochastic security: Adversarial defense using long-run dynamics of energy-based models, arXiv preprint arXiv:2005.13525 (2020).
 - [5] D. H. Ackley, G. E. Hinton, and T. J. Sejnowski, A learning algorithm for Boltzmann machines, *Cognitive science* **9**, 147 (1985).
 - [6] J. J. Hopfield, Neural networks and physical systems with emergent collective computational abilities, *Proceedings of the national academy of sciences* **79**, 2554 (1982).

- [7] G. E. Hinton, S. Osindero, and Y.-W. Teh, A fast learning algorithm for deep belief nets, *Neural computation* **18**, 1527 (2006).
- [8] G. E. Hinton, Learning multiple layers of representation, *Trends in cognitive sciences* **11**, 428 (2007).
- [9] D. Koller and N. Friedman, *Probabilistic graphical models: principles and techniques* (MIT press, 2009).
- [10] P. Clifford and J. Hammersley, Markov fields on finite graphs and lattices, (1971).
- [11] E. Nijkamp, M. Hill, T. Han, S.-C. Zhu, and Y. N. Wu, On the anatomy of MCMC-based maximum likelihood learning of energy-based models, in *Proceedings of the AAAI Conference on Artificial Intelligence*, Vol. 34 (2020) pp. 5272–5280.
- [12] T. Che, R. Zhang, J. Sohl-Dickstein, H. Larochelle, L. Paull, Y. Cao, and Y. Bengio, Your GAN is secretly an energy-based model and you should use discriminator driven latent sampling, *Advances in Neural Information Processing Systems* **33**, 12275 (2020).
- [13] T. Chen, E. Fox, and C. Guestrin, Stochastic gradient Hamiltonian Monte Carlo, in *International conference on machine learning* (PMLR, 2014) pp. 1683–1691.
- [14] E. Nijkamp, M. Hill, S.-C. Zhu, and Y. N. Wu, Learning non-convergent non-persistent short-run mcmc toward energy-based model, *Advances in Neural Information Processing Systems* **32** (2019).
- [15] B. M. Terhal and D. P. DiVincenzo, Problem of equilibration and the computation of correlation functions on a quantum computer, *Physical Review A* **61**, 022301 (2000).
- [16] D. Poulin and P. Wocjan, Sampling from the thermal quantum gibbs state and evaluating partition functions with a quantum computer, *Physical review letters* **103**, 220502 (2009).
- [17] K. Temme, T. J. Osborne, K. G. Vollbrecht, D. Poulin, and F. Verstraete, Quantum metropolis sampling, *Nature* **471**, 87 (2011).
- [18] M. J. Kastoryano and F. G. Brandao, Quantum gibbs samplers: the commuting case, *Communications in Mathematical Physics* **344**, 915 (2016).
- [19] A. N. Chowdhury and R. D. Somma, Quantum algorithms for Gibbs sampling and hitting-time estimation, *Quantum Info. Comput.* **17**, 41–64 (2017).
- [20] J. van Apeldoorn, A. Gilyén, S. Gribling, and R. de Wolf, Quantum sdp-solvers: Better upper and lower bounds, in *Foundations of Computer Science (FOCS), 2017 IEEE 58th Annual Symposium on* (IEEE, 2017) pp. 403–414.
- [21] J. Lemieux, B. Heim, D. Poulin, K. Svore, and M. Troyer, Efficient quantum walk circuits for metropolis-hastings algorithm, *Quantum* **4**, 287 (2020).
- [22] N. Wiebe, A. Kapoor, and K. M. Svore, Quantum deep learning, arXiv preprint arXiv:1412.3489 (2014).
- [23] M. H. Amin, E. Andriyash, J. Rolfe, B. Kulchytskyy, and R. Melko, Quantum boltzmann machine, *Physical Review X* **8**, 021050 (2018).
- [24] D. Crawford, A. Levit, N. Ghadermarzy, J. S. Oberoi, and P. Ronagh, Reinforcement learning using quantum boltzmann machines, arXiv preprint arXiv:1612.05695 (2016).
- [25] A. Levit, D. Crawford, N. Ghadermarzy, J. S. Oberoi, E. Zahedinejad, and P. Ronagh, Free energy-based reinforcement learning using a quantum processor, arXiv preprint arXiv:1706.00074 (2017).
- [26] B. Sepehry, E. Iranmanesh, M. P. Friedlander, and P. Ronagh, Quantum algorithms for structured prediction, arXiv preprint arXiv:1809.04091 (2018).
- [27] A. M. Childs, T. Li, J.-P. Liu, C. Wang, and R. Zhang, Quantum algorithms for sampling log-concave distributions and estimating normalizing constants, arXiv preprint arXiv:2210.06539 (2022).
- [28] A. Motamedi and P. Ronagh, Gibbs sampling of periodic potentials on a quantum computer, arXiv preprint arXiv:2210.08104 (2022).
- [29] G. A. Pavliotis, *Stochastic processes and applications: diffusion processes, the Fokker-Planck and Langevin equations*, Vol. 60 (Springer, 2014).
- [30] C. Guo, G. Pleiss, Y. Sun, and K. Q. Weinberger, On calibration of modern neural networks, in *International Conference on Machine Learning* (PMLR, 2017) pp. 1321–1330.
- [31] S. Zagoruyko and N. Komodakis, Wide residual networks (2016).
- [32] M. A. Nielsen and I. Chuang, Quantum computation and quantum information (2002).
- [33] A. Krizhevsky, *Learning multiple layers of features from tiny images*, Tech. Rep. (2009).
- [34] T. Tieleman and G. Hinton, Using fast weights to improve persistent contrastive divergence, in *Proceedings of the 26th annual international conference on machine learning* (2009) pp. 1033–1040.
- [35] D. P. Kingma and J. Ba, Adam: A method for stochastic optimization, (2014), cite arxiv:1412.6980 Comment: Published as a conference paper at the 3rd International Conference for Learning Representations, San Diego, 2015.
- [36] A. Madry, A. Makelov, L. Schmidt, D. Tsipras, and A. Vladu, Towards deep learning models resistant to adversarial attacks, arXiv preprint arXiv:1706.06083 (2017).
- [37] A. Athalye, N. Carlini, and D. Wagner, Obfuscated gradients give a false sense of security: Circumventing defenses to adversarial examples, in *International conference on machine learning* (PMLR, 2018) pp. 274–283.
- [38] Defense Advanced Research Projects Agency (DARPA), Quantifying utility of quantum computers, Retrieved April 16, 2023, from <https://www.darpa.mil/news-events/2021-04-02> (2021), accessed on April 16, 2023.
- [39] J. Ho, A. Jain, and P. Abbeel, Denoising diffusion probabilistic models, *Advances in Neural Information Processing Systems* **33**, 6840 (2020).
- [40] R. Desislavov, F. Martínez-Plumed, and J. Hernández-Orallo, Compute and energy consumption trends in deep learning inference, arXiv preprint arXiv:2109.05472 (2021).
- [41] P. Li, J. Yang, M. A. Islam, and S. Ren, Making AI less thirsty: Uncovering and addressing the secret water footprint of AI models, arXiv preprint arXiv:2304.03271 (2023).